Functional modulation of power-law distribution in visual perception

Masanori Shimono,[1] Takashi Owaki,[1] Kaoru Amano,[2] Keiichi Kitajo,[3] and Tsunehiro Takeda[1]
[1]*Laboratory for Biological Complex Systems, Department of Complexity Science and Engineering, Graduate School of Frontier Science, The University of Tokyo, 5-1-5, Kashiwanoha, Kashiwa-shi, Chiba 277-8561, Japan*
[2]*Sensory and Motor Research Group, Human and Information Science Laboratory, NTT Communication Science Laboratories, 3-1, Morinosato Wakamiya Atsugi-shi, Kanagawa 243-0198, Japan*
[3]*Laboratory for Dynamics of Emergent Intelligence, RIKEN, Brain Science Institute, 2-1, Hirosawa, Wako, Saitama 351-0198, Japan*
(Received 1 September 2006; revised manuscript received 6 January 2007; published 4 May 2007)

Neuronal activities have recently been reported to exhibit power-law scaling behavior. However, it has not been demonstrated that the power-law component can play an important role in human perceptual functions. Here, we demonstrate that the power spectrum of magnetoencephalograph recordings of brain activity varies in coordination with perception of subthreshold visual stimuli. We observed that perceptual performance could be better explained by modulation of the power-law component than by modulation of the peak power in particular narrow frequency ranges. The results suggest that the brain operates in a state of self-organized criticality, modulating the power spectral exponent of its activity to optimize its internal state for response to external stimuli.

DOI: 10.1103/PhysRevE.75.051902 PACS number(s): 87.19.La, 05.45.Tp, 05.65.+b, 87.19.Dd

I. INTRODUCTION

Synchronous neural oscillations are prominent features of human brain activity and are thought to play a significant role in cognitive functions [1]. When the functional roles of such oscillations are being considered, their frequencies are commonly categorized into bands $\delta, \theta, \alpha, \beta, \gamma$ [Fig. 1(a)], and most studies on the relationship between neural activities and cognitive functions [2,3] have focused on band-specific neural activity. However, neural activities in subjects at rest, that is, when not responding to external stimuli, have been frequently reported to exhibit a broad-band power-law distribution with a scale-free property [4–6]. Moreover, even in subjects actively responding to external stimuli neuronal activities can exhibit a power-law distribution [Fig. 1(a)]. The relationship of such distributions to cognitive function, however, remains unknown. One possibility is that the observed power-law distributions arise from a state of self-organized criticality (SOC) in the brain, and that this state is maintained by the brain in order to optimize cognitive function.

SOC [7–10], a concept in complexity physics that has been studied in the context of a wide range of fields including geophysics, economics and biology, also has been characterized in the context of the brain's neural oscillations. SOC generally refers to a mechanism of slow energy accumulation and fast energy redistribution that drives the system toward a critical state wherein the spatiotemporal distribution of elements in the system, interconnected nonlinearly, exhibit power-law scaling behavior without fine-tuning. Recent studies have done well at accounting for the spectral exponent of the power distribution, observed using noninvasive brain measurement techniques such as Electroencephalography (EEG), magnetoencephalography (MEG), or functional magnetic resonance imaging (fMRI), using theoretical models of the SOC state [8,11,12]. However, in these studies, subjects were at rest and were simply requested either to open or to close their eyes.

Intriguingly, it is known that artificial neural networks in the SOC state are highly sensitive to weak external perturbations [13–15]. This property could render SOC in the neural networks of the brain an optimal state for detecting weak stimuli. Therefore, we expected that the power-law component (PLC) of the spectral distribution of brain activity could be closely related to the perception of weak external stimuli.

Recently, it has been demonstrated that modulation in α band power in the MEG signal shows power-law scaling behavior, and also that SOC plays an important role in detecting weak somatosensory stimuli [16–18]. However, the power-law behavior discussed in these previous studies was limited to the modulation of the peak power only in a few specific frequency bands. In contrast, we investigated the possible functional roles of power-law scaling behavior across a wide frequency range without being limited by *a priori* assumptions regarding the functional roles of particular frequency bands in perception or cognition. Here we report experimental results demonstrating that perceptual performance can be explained better by variations in the PLC of

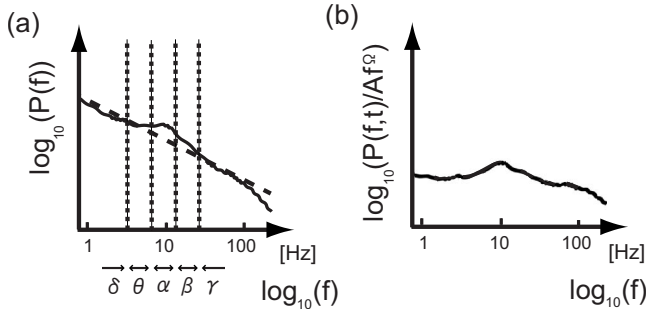

FIG. 1. (a) A representative wavelet power spectrum of a magnetic field on the surface of a human head, measured with MEG (black solid line). The subject was presented with weak flickering visual stimuli. The power spectrum approximately obeys a power law (dashed line). Dotted lines demarcate the five frequency bands δ(1.5–3.5 Hz), θ(3.5–6.5 Hz), α(7.0–13 Hz), β(15–30 Hz), γ($\geq$30 Hz). (b) Residual component after subtraction of the power-law component (PLC) from the raw wavelet power spectrum.

raw MEG data than by variations in peak power of particular frequency components of those data.

We compared three models of modulations of the wavelet power spectrum (WPS). In model 1, perceptual performance is assumed to correlate with peak amplitudes in particular frequency ranges (model 1). In model 2, perceptual performance is assumed to correlate with two parameters, spectral exponent Ω and intensity A in a power-law distribution described by $Af^{-\Omega}$. These parameters are obtained by fitting the distribution function $Af^{-\Omega}$ to each time point of $P(f,t)$ (model 2). In model 3, perceptual performance is assumed to correlate with certain peak intensities in specific frequency components in the residual power spectrum $P(f,t)/Af^{-\Omega}$ after subtracting the PLC from the raw power spectrum on a log scale (model 3). We compared models 1 and 3 to confirm the importance of the PLC (model 2) in the explanation of behavioral performance before directly comparing model 1 and model 2.

II. PREPARATION AND METHOD

Seven healthy males (23–26 yr) participated in the experiment after giving informed consent [19]. We investigated their performance in detecting a flickering visual stimulus in the dark. In this experiment, brain magnetic fields were recorded in a magnetically shielded room using a wholehead MEG system (PQ2440R; Yokogawa, Tokyo, Japan) with 440 gradiometers. The sampling frequency of MEG was 500 Hz, and the signals were bandpass filtered between 0.03 and 200 Hz. The size of the screen was $40° \times 30°$. A fixation cross with a 3° diagonal was located at the center of the screen and a target stimulus flickering at 10 Hz was presented in the lower left or lower right visual fields [Figs. 2(a) and 2(c)]. Before the main experiment, we measured the detection threshold (step 1) and identified responsive sensors for each stimulus position (step 2).

In step 1, the target stimulus was presented at one of the two possible target locations randomly and stimulus intensity was changed to one of 6 levels in randomized order. Subjects were asked to press one of the two buttons with their right index finger when they detected the target in the left visual field, and with their right middle finger when they detected it in the right visual field. Each subject performed 200 trials. The time course of the stimulus is shown in Fig. 2(a). The integral of the Gaussian probability density function was fitted to the averaged proportions of correct responses of the six brightness levels by the least-squares method [Fig. 2(b)]. The brightness of the target stimulus was adjusted to the 75% level of correct detections on the fitted curve for each subject in the main experiment. In step 2, subjects were presented with a flickering stimulus either in the lower right or lower left visual fields, respectively, 350 times [Fig. 2(c)]. From the resulting data we identified six planar gradiometers that showed a strong evoked response at around 100 ms after stimulus onset. The electrical current source in the primary visual cortex was estimated by applying the steepest descent method for the magnetic field of all axial gradiometers [Fig. 2(d)] [20]. This technique was used because the peak response around 100 ms strongly correlates with contrast-detection performance [21].

In the main experiment, we performed a similar experiment as in step 1, setting the stimulus intensity at the 75%-correct detection threshold. We applied a wavelet transform to extract information about the MEG power spectrum from the six sensors chosen in step 2, using the Morlet wavelet as the mother wavelet [Eq. (1)].

$$w(t,f_0) = \frac{1}{\sqrt{\sigma_t\sqrt{\pi}}} \exp\left(-\frac{t}{2\sigma_t^2}\right)\exp(2i\pi f_0), \qquad (1)$$

where σ_t is the variance along the time axis and f_0 represents the center frequency. σ_t is defined as five times the size of the period $1/f_0$. To confirm that there was no artificial correlation over wide frequency ranges, we analyzed the WPS obtained from harmonic artificial data in 1–40 Hz with the same wavelet and verified that the maximum value of variance was not over 2.5 Hz. We analysed trials remaining after artifact rejection combined over all subjects. Artifacts, including blinks, eye movements, and muscle movements were rejected using an amplitude criterion (2.0 [pT]) in the stimulus period. Then we categorized all the trials into correct and incorrect, and compared their WPSs. The total number of trials analyzed was about 1200 (174±16 for each subject).

III. RESULTS OF WAVELET ANALYSES

Figure 3 shows the average WPS obtained across all subjects and all trials from the left occipital sensors when the stimulus was in the right visual field. Figure 3(a) shows the mean difference in the raw WPS between the correct and incorrect trials. Similarly, Fig. 3(b) demonstrates the difference calculated for residual WPS derived by subtracting the PLC from raw WPS for each trial. The PLC was obtained by fitting data points between 0.1 and 37 Hz by the method of least squares. We chose this frequency range because the power supply noise (60 Hz) and its higher harmonics were observed in the MEG signal when subjects were not in the shielded room. We performed a two-tailed t test, with p values less than 0.05 considered significant, to test for differences between correct and incorrect trials for measures of WPS, such as the spectral exponent and raw WPS and residual WPS at each point in the time-frequency space. First, we compared the results of statistical tests for the WPS based on model 1 and those based on model 3 [Figs. 3(c) and 3(d)]. There was an area where significant differences were observed in model 1 but not in model 3. This means that the subtracted PLC includes a significant difference between correct and incorrect trials.

Next, to examine how the differences in WPS between correct and incorrect trials can be explained by model 2, which assumes two parameters, spectral exponent and intensity A, we focused on three time ranges A, B, and C, in which the two groups of trials showed significant differences [Fig. 3(c)]. In time window A, the WPS of the middle frequency components α and β were significantly different between correct and incorrect trials. Since the spectral exponent showed significant differences between the correct and incorrect trials only in a short time period within window A [Fig. 3(e)], the differences in WPS cannot be explained solely by

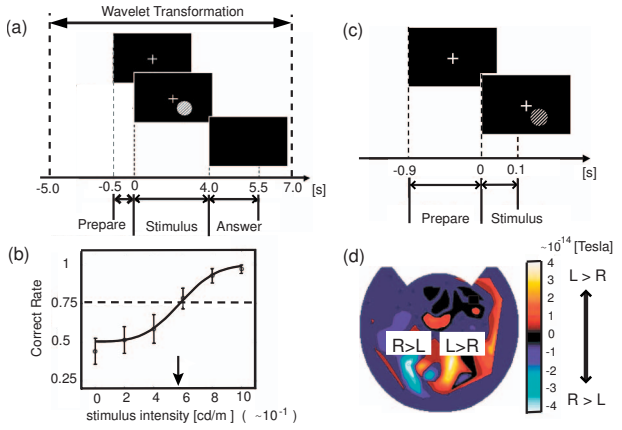

FIG. 2. (Color) (a) Time course of the stimulus presented to identify the detection threshold. (b) Relationship between stimulus amplitude and probability of correctly detecting the stimulus obtained from one subject. Error bars correspond to SD. A probability of 0.75 (dotted line) defined the detection threshold (arrow). (c) Time course of the stimulus for selection of sensors, which show activity depending on the stimulus position. (d) The difference between magnetic fields activated by a stimulus presented in the lower left and lower right visual fields. Positive (negative) areas are those in which neural activity was stronger (weaker) when the stimulation was in the left visual field than when it was in the right visual field.

modulation of the spectral exponent. To understand this phenomenon, we analyzed the cooperative modulation of the power in pairs of frequency bands (e.g., α and β) by calculating the product between averages of

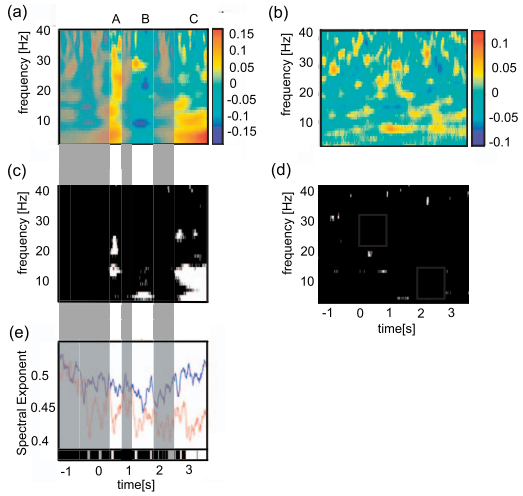

FIG. 3. (Color) (a) Difference in mean WPS between correct and incorrect trials. (b) The mean difference for data set across all subjects in the residual WPS between the correct and incorrect trials. The residual WPS are obtained by subtracting PLC from the raw power spectrum for each trial. (c) Statistically significant difference in mean WPS in (a). Areas with significant differences are shown in white (two-tailed t test with Bonferroni correction; $p<0.005$). (d) Statistically significant difference in the residual WPS in (b) ($p<0.005$). (e) Time courses of the averaged spectral exponents on correct (blue) and incorrect trials (red). Binary color map below time courses shows the results of a two-tailed t test for spectral exponents ($p<0.005$).

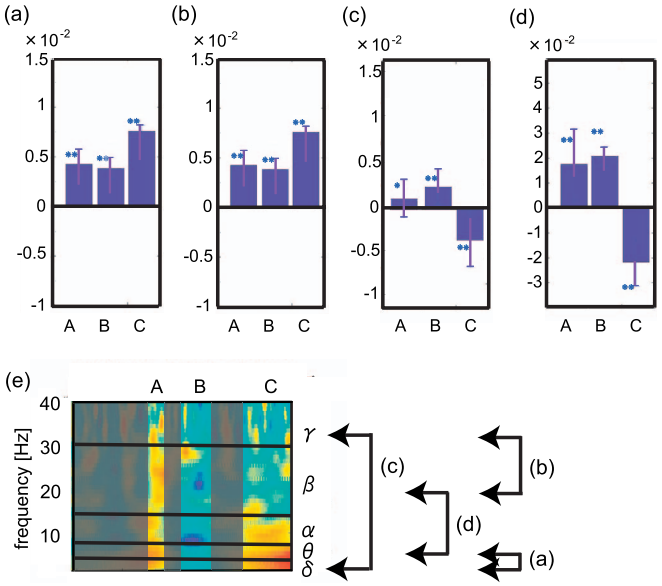

FIG. 4. (Color) Products of WPS modulations of frequency bands (a) δ and θ, (b) β and γ, (c) δ and γ, and (d) θ and β in time windows A, B, and C. Error bars correspond to SD. (e) Pairs of frequency components shown in (a)–(d). Statistical test is performed in each time-frequency window by comparing the averaged WPS for correct trials and that for incorrect trials (two-tailed t test, $*;p<0.05$, $**;p<0.01$).

$$M(f,t)=\log_{10}[\tilde{P}_{\mathrm{cor}}(f,t)/\tilde{P}_{\mathrm{incor}}(f,t)] \tag{2}$$

across frequencies within the two frequency ranges at each time point, where $\tilde{P}_{\mathrm{cor}}(f,t)$ and $\tilde{P}_{\mathrm{incor}}(f,t)$ is the average power at frequency f on correct and incorrect trials, respectively (Fig. 4). Then, we calculated the products between mean power in one frequency range and that in the other frequency range at each time section, and tested whether the data set of products in each time window were significantly different from zero (two-tailed t test). In window A, the products had positive values in all pairs of frequency bands in

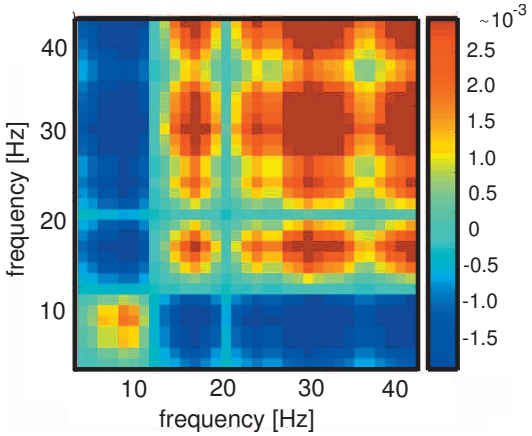

FIG. 5. (Color) The contour map for the average of the product between $M(f_1,t)$ and $M(f_2,t)$ in time window C. Here, f_1 and f_2 are two frequencies. Yellow and red areas indicate positive values, and blue areas indicate negative values, of the average product.

Figs. 4(a)–4(d). In other words, the WPSs in all frequency bands in this window are different in the same direction when comparing incorrect to correct trials. Moreover, in Fig. 3(a), the direction is positive and the modulations do not show remarkable peaks in specific frequency bands but spread continuously over a wide frequency domain. Only the α and β frequency bands showed a significant difference ($p<0.005$). When increasing the p value to 0.05, however, the δ, θ and γ bands also showed significant differences (data not shown).

In window B, all products of WPS in the various frequency bands also had positive values. Figure 3(a) shows that WPS in all frequency bands in window B are modulated negatively from incorrect trials to correct ones. On the other hand, in window C, the products between low frequency bands such as δ and θ, and high frequency bands such as β and γ, showed positive values, while products between one low frequency and one high frequency band showed negative values (Fig. 4). In addition, spectral exponents for correct and incorrect trials also showed significant differences in window C [Fig. 3(e)]. To detect a fixed frequency point in the modulation of PLC in window C on the frequency axis consecutively, we evaluated the modulation of PLC by the product between $M(f_1,t)$ and $M(f_2,t)$. Here f_1 and f_2 are two specific frequencies. The averaged values of the products in window C were then presented as a contour map (Fig. 5).

In Fig. 5, in window C, products of only low frequency bands and also those of only high frequency bands have positive values, while those of low frequency with high frequency bands have negative values, the sign reversing at around 13 Hz. These results suggest that 13 Hz is a fixed point for the modulation of the spectral exponent. A part of the modulation may correspond to the significant differences in the low frequency range in the above results based on model 1 [Fig. 3(a)]. This interpretation is strongly supported by two facts: (1) changing the significance level of the p value from 0.01 to 0.05 renders the differences in high frequency ranges, such as β and γ, significant, and (2) the p values for the entire data set of all points included in each time-frequency window are as low as 0.005 (data not shown).

IV. DISCUSSION

In summary, two features stand out in three time windows during which, over some frequency ranges, there were significant differences in WPS between correct and incorrect trials [Fig. 3(c)]. The first feature is that the WPS in all frequency ranges is modulated in the same direction, either positive or negative in windows A and B. The second one is that the WPS in low and high frequency ranges are modulated in the opposite direction in window C. Furthermore, in the first case, WPS around the frequency boundaries, which is about 13 Hz between the α and β bands, is modulated as strongly as WPS within these frequency ranges. This clearly shows that the modulation opposes the band-specific activity model, model 1.

The most prominent feature of Fig. 3(c) is that "specific" frequency components look activated. However, considering that peak activities are eliminated by subtraction of PLC, and the two features just described from the above analyses, the difference between correct and incorrect behavioral performance can be explained better by the modulation of widely distributed PLC than by narrow peak activities in particular frequency ranges. In similar previous experimental studies, brain activities were measured only in resting states without external stimulation [4,5]. In this paper, however, we suggest that the modulation of the power-law component affected performance in detecting a weak visual stimulus. Our results are consistent with the results of previous theoretical studies showing that the neural networks in the SOC state show high sensitivity to small environmental changes [13–15]. Our results suggest that the fixed point for modulation of the spectral exponent is around 13 Hz. However, further research must be performed to understand the reason for this specific value. In the present research, remarkable modulations of the amplitude and of the spectral exponent in the power distribution model were observed in different time windows. However, in the general case, we must apply an appropriate analytical method not only to differentiate the effects of these components, but also to differentiate the effects of the PLC from those of peak activity [22]. Our results suggest that PLC plays a major role in the brain activity reflecting perception of weak stimuli around detection threshold, making the concept of SOC seem applicable to the maintenance of optimal neural activity for perception and cognition.

ACKNOWLEDGMENTS

We are grateful to Professor Yoshiharu Yamamoto and Dr. Kentaro Yamanaka for fruitful discussion, and to Professor Lawrence M. Ward for detailed comments for this report.

[1] *Electroencephalography: Basic Principles, Clinical Applications, and Related Fields*, edited by E. Niedermeyer and F. H. Lopes da Silva (Williams and Wilkins, Baltimore, 1998).
[2] W. Klimesch, Brain Res. Rev. **29**, 169 (1999).
[3] E. Basar, C. B-. Eroglu, S. Karakas, and M. Schurmann, Neurosci. Lett. **259**, 165 (1999).
[4] C. J. Stam and E. A. Bruin, Hum. Brain Mapp **22**, 97 (2004).
[5] E. Novikov, A. Novikov, D. Shannahoff-Khalsa, B. Schwartz, and J. Wright, Phys. Rev. E **56**, R2387 (1997).
[6] V. G. Kiselev, K. R. Hahn, and D. P. Auer, Neuroimage **20**, 1765 (2003).
[7] P. Bak, C. Tang, and K. Wiesenfeld, Phys. Rev. Lett. **59**, 381 (1987).
[8] L. deArcangelis, C. Perrone-Capano, and H. J. Herrmann, Phys. Rev. Lett. **96**, 028107 (2006).
[9] P. Bak, C. Tang, and K. Wiesenfeld, Phys. Rev. A **38**, 364 (1988).
[10] J. M. Beggs and D. Plenz, J. Neurosci. **23**, 11167 (2003).
[11] P. A. Robinson, C. J. Rennie, J. J. Wright, H. Bahramali, E. Gordon, and D. L. Rowe, Phys. Rev. E **63**, 021903 (2001).

[12] V. M. Eguiluz, D. R. Chialvo, G. A. Cecchi, M. Baliki, and A. V. Apkarian, Phys. Rev. Lett. **94**, 018102 (2005).
[13] P. Alstrom and D. Stassinopoulos, Phys. Rev. E **51**, 5027 (1995).
[14] D. Stassinopoulos and P. Bak, Phys. Rev. E **51**, 5033 (1995).
[15] D. R. Chialvo and P. Bak, Neuroscience **90**, 1137 (1999).
[16] K. Linkenkaer-Hansen, V. V. Nikouline, J. M. Palva, and R. J. Ilmoniemi, J. Neurosci. **21**, 1370 (2001).
[17] K. Linkenkaer-Hansen, V. V. Nikouline, J. M. Palva, K. Kaila, and R. J. Ilmoniemi, Eur. J. Neurosci. **19**, 203 (2004).
[18] K. Linkenkaer-Hansen, V. V. Nikouline, J. M. Palva, R. J. Ilmoniemi, and J. M. Palva, J. Neurosci. **24**, 10186 (2004).
[19] I. Hashimono, R. Kakigi, T. Nagamine, N. Nakasato, H. Shiraishi, and Y. Watanabe, J. Clin. Neurophysiol. **33**, 4 (2005).
[20] The SQUID gradiometers of our MEG system consist of 300 axial gradiometers ($\delta B_z/\delta z$) and 70×3 planar gradiometers ($\delta B_x/\delta z, \delta B_y/\delta z$). The axes of $\delta B_z/\delta z$ sensors' circuits are in vertical alignment with the scalp, and the axes of $\delta B_x/\delta z$ and $\delta B_y/\delta z$ sensors' circuits are horizontal to it. Therefore, the magnetic field map measured with $\delta B_z/\delta z$ sensors shows a negative peak and a positive peak for one dipole electrical current source (ECS) running parallel to the scalp. However, these peaks are not necessarily located near the ECS. On the other hand, the root mean square (rms) value of $\delta B_x/\delta z$ and $\delta B_y/\delta z$ sensors can detect the electrical current immediately below them.
[21] J. D. Haynes, G. Roth, M. Stadler, and H. J. Heinze, J. Neurosci. **89**, 2655 (2003).
[22] Y. Yamamoto and R. L. Hughson, Physica D **68**, 250 (1993).